J. Fluid Mech. (1994), *vol.* 277, *pp.* 303–329

Thermocapillary convection and existence of continuous liquid layers in the absence of gravity

By J. M. FLORYAN AND C. CHEN

Department of Mechanical Engineering, The University of Western Ontario, London, Ontario, N6A 5B9, Canada

(Received 1 December 1992 and in revised form 10 May 1994)

Thermocapillary convection in an infinite liquid layer driven by a temperature gradient parallel to the interface in the absence of gravity is considered. It is demonstrated that the temperature field has to satisfy restrictive conditions in order for a continuous layer to exist. It is further shown that the same conditions apply to long finite layers. Such layers, when subject to heating that does not satisfy the existence conditions, undergo large deformations and possible break up if the layer is sufficiently long.

1. Introduction

Thermocapillary convection has been recognized as an important transport mechanism in many areas of technology, such as zero-gravity containerless materials processing, where it is a dominant source of motion, or in conventional crystal growth and welding processes, where it is a contributing factor. Control and optimization of these processes, particularly for zero-gravity applications, critically depend on the complete understanding of all phenomena that may be induced by the thermocapillary effect.

The objective of this work is to study phenomena induced by the thermocapillary effect in a liquid layer in the absence of gravity. This configuration has been selected owing to its simple geometrical form. The layer is resting on a solid plate and its upper free surface (see figure 1) is subject to an arbitrary external heating. Since the temperature gradient vector is parallel to the interface, the thermocapillary effect always generates some motion, regardless of the magnitude of the temperature gradient. This is in contrast to the more classical case of Marangoni instability, where the temperature gradient is normal to the interface and motion does not begin until certain critical conditions are met.

Two types of layers, i.e. infinite (figure 1) and finite (figure 2), have been selected for the analysis. Their comparison allows us to estimate the importance of geometrical constraints (sidewalls, contact conditions) on the convection inside the layer and on the deformation of the interface.

The subject of thermocapillary convection in infinite layers has been considered before under a variety of simplifying assumptions. Levich (1962) and Birikh (1966) analysed a two-dimensional layer with a non-deformable interface and flow being parallel to the boundaries. The resulting solution did not satisfy the condition of constant pressure along the interface. Yih (1968) reconsidered this problem in the context of chemico-capillary flows with gravity present and with allowance for small interface deformation. Sanochkin (1983) considered the interface to be flat and included transverse velocity components with simplifying assumptions analogous to those used in boundary-layer theory. Lai & Chai (1986) carried out an assessment of

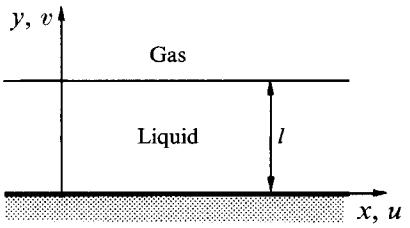

FIGURE 1. Schematic diagram of liquid layer.

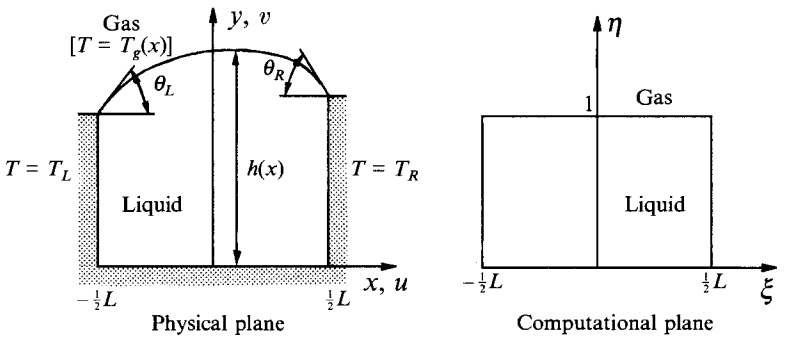

FIGURE 2. Schematic diagram of liquid in a cavity and its computational model.

convective heat transport effects under similar assumptions. Sanochkin (1984) evaluated inertial effects and Vybornov & Sanochkin (1985) analysed small interface distortions. Pshenichnikov & Tokmenina (1983) demonstrated experimentally that an appreciable curving of the interface occurs when the thickness of the layer is sufficiently small. Adler & Sowerby (1970) extended Yih's (1968) analysis into three dimensions. Pimputkar & Ostrach (1980) considered transient flow induced by a fixed interface temperature with the flow being, in effect, parallel to the interface and inertial effects being negligible. Kopbosynov & Pukhnachev (1986) extended this approach to three-dimensional situations.

Thermocapillary convection in finite cavities has also attracted a lot of attention. Sen & Davis (1982) considered flow in a very long cavity driven by a linear temperature distribution with capillary number decreasing inversely proportionally to the cavity length. Sen (1986) reconsidered this problem and allowed large interface deformations to occur. Numerical simulations for various combinations of Reynolds, Prandtl, Marangoni and Biot numbers and different external heating have been carried out by numerous authors (Rivas & Ostrach 1989; Hadid & Roux 1992; Laure, Roux & Hadid 1990; Hadid & Roux 1990; Carpenter & Homsy 1990; Rivas 1991; Zebib, Homsy & Meiberg 1985; Cowley & Davis 1983). The interface was always assumed to be essentially non-deformable, which limited the scope of these studies to the analysis of the convention patterns only.

The purpose of the present work is to carry out a complete analysis of the response of a liquid layer to external heating. It will be demonstrated that the dominant part of this response consists of large interfacial distortions (and possible breakup), and not of convection, as commonly assumed. Small deformations may occur only if the external temperature field satisfies a set of very restrictive existence conditions. The form of these conditions shows that it may not be possible to satisfy them in most practical applications. The analysis will be carried out without any simplifying assumptions in

order to demonstrate the generality of the existence conditions. A set of carefully selected examples will be used to illustrate response of the layer to various types of external heating and to show that the layer, if sufficiently long, will break up when exposed to heating that violates the existence conditions.

Similar existence conditions can be identified in the case of liquid layers driven by other means, e.g. chemico-capillary flows. This class of flows has been studied by Homsy & Meiburg (1984) and Carpenter & Homsy (1985) using assumptions similar to those used by Sen & Davis (1982).

The paper is organized as follows. Section 2 gives the formulation of the flow problem. Section 3 presents the solution with the small-interface-deformation assumption and describes conditions under which such deformation may exist. Section 4 discusses general solutions with an arbitrary deformation. Section 5 describes interface diagnostic procedures. Section 6 provides short summary of the main conclusions.

2. Problem formulation

Consider a liquid layer of thickness l, infinite in the x-direction, bounded by a solid insulated plate from below and a gas from above, as shown in figure 1. The liquid is incompressible, Newtonian, has density ρ, thermal conductivity k, specific heat per unit mass c, thermal diffusivity $\kappa = k/\rho c$, kinematic viscosity ν and dynamic viscosity μ. The free surface, described by $y = h(x)$, is bounded by a passive gas of negligible density and viscosity. This free surface is associated with a surface tension σ, which depends on the local temperature. It is assumed, without loss of generality, that the pressure of the gas is negligible.

In the absence of gravity, the steady motion of the liquid is governed by the continuity, Navier–Stokes and energy equations subject to the following boundary conditions:

$$y = 0: \quad U = T_y = 0, \tag{2.1a}$$

$$F(x,y) = y - h(x) = 0: \quad \boldsymbol{U}\cdot\boldsymbol{\nabla}F = 0 \tag{2.1b}$$

$$\boldsymbol{S}\cdot\boldsymbol{n} = 2\sigma\Lambda\boldsymbol{n} + \sigma_s\boldsymbol{t} \tag{2.1c}$$

$$k\boldsymbol{\nabla}T\cdot\boldsymbol{n} + H(T - T_g) = 0. \tag{2.1d}$$

In the above, $\boldsymbol{U} = u\boldsymbol{i} + v\boldsymbol{j}$ is the velocity vector, $\boldsymbol{i}$ and $\boldsymbol{j}$ are the unit vectors in the x- and y-directions, respectively, T is the temperature of the liquid, $\boldsymbol{S}$ is the stress tensor of the liquid, Λ stands for the mean curvature of the interface, $\boldsymbol{\nabla}$ denotes the nabla operator, $\boldsymbol{n}$ stands for the unit vector normal to the interface pointing outwards, $\boldsymbol{t}$ denotes the unit vector tangential to the interface, the subscripts x, y denote partial derivatives $\partial/\partial x$, $\partial/\partial y$, respectively, and the subscripts n, s denote normal and tangential derivatives at the interface, respectively.

Equation (2.1*b*) is the kinematic condition at the liquid–gas interface. The stress balances at the interface are given by (2.1*c*). The jump in the normal stress across the interface is balanced by the surface tension times the mean curvature, and the jump in the shear stress at the interface is balanced by the surface tension gradient. The unit vectors are defined as follows:

$$\boldsymbol{n} = (-h_x\boldsymbol{i} + \boldsymbol{j})/N, \quad \boldsymbol{t} = (\boldsymbol{i} + h_x\boldsymbol{j})/N, \tag{2.2}$$

where

$$N = (1 + h_x^2)^{1/2}. \tag{2.3}$$

The mean curvature Λ of the interface in (2.1*c*) has the definition

$$\Lambda = -\tfrac{1}{2}\boldsymbol{\nabla}\cdot\boldsymbol{n} = \tfrac{1}{2}h_{xx}N^{-3}. \tag{2.4}$$

The thermal boundary condition at the interface is given by (2.1 d) in which k is the thermal conductivity of the liquid, H is the heat transfer coefficient in the gas and $T_g(x)$ is the temperature in the gas phase. The thermal boundary condition presumes that the gas temperature $T_g(x)$ is known *a priori* and that the heat transport at the liquid–gas interface can be described by using a heat-transfer coefficient H.

Apart from boundary conditions (2.1), the liquid must also satisfy the mass conservation constraint. Since the liquid is assumed to be incompressible, its total volume must remain constant, i.e.

$$\text{volume} = \text{const.} \tag{2.5}$$

Solution to the problem requires specification of the type of behaviour of the interface as $x \to \pm\infty$. Two cases will be considered, i.e.

$$h < D, \qquad h_x \to 0 \tag{2.6a, b}$$

where D is an arbitrary constant. Condition (2.6a) states that the interface remains bounded as $x \to \pm\infty$ and is less restrictive than (2.6b) which requires that the interface becomes flat as $x \to \pm\infty$.

We shall use a linear equation of state for surface tension. In particular, we take

$$\sigma(T) = \sigma_* - \gamma(T - T_*), \tag{2.7}$$

where σ_* is the surface tension of the liquid at the reference temperature T_* and the constant γ is the negative of the derivative of the surface tension with respect to temperature.

We scale the problem by using l, u_*, $\mu u_*/l$ and σ_* as the length, velocity, pressure and surface tension scales, respectively. The dimensionless temperature T' is defined as

$$T - T_* = (T_{max} - T_{min})\, T', \quad T_g - T_* = (T_{max} - T_{min})\, T'_g. \tag{2.8}$$

Here T_{max} and T_{min} denote a measure of the maximum and the minimum of the interface temperature, respectively. The characteristic velocity u_* is derived from the so-called Marangoni effect, i.e. the jump in shear along the interface balances the surface tension gradient. This leads to

$$u_* = \gamma(T_{max} - T_{min})/\mu. \tag{2.9}$$

With the above definitions the dimensionless equations (with the primes dropped) can be written in the form

$$L_1(u, v) \equiv \nabla \cdot \boldsymbol{U} = 0, \tag{2.10a}$$

$$\boldsymbol{L}_2(u, v, p) \equiv Re(\boldsymbol{U} \cdot \nabla)\, \boldsymbol{U} + \nabla p - \nabla^2 \boldsymbol{U} = 0, \tag{2.10b}$$

$$L_3(u, v, T) \equiv Ma(\boldsymbol{U} \cdot \nabla)\, T - \nabla^2 T = 0, \tag{2.10c}$$

where p denotes the pressure.

Reynolds number Re and Maragoni number Ma have the standard definitions, i.e.

$$Re = \frac{u_* l}{\nu} = \frac{\gamma(T_{max} - T_{min})\, l}{\mu\nu}, \qquad Ma = \frac{u_* l}{\kappa} = \frac{\gamma(T_{max} - T_{min})\, l}{\mu\kappa}. \tag{2.11}$$

The boundary conditions (2.1) transforms to

$$y = 0: \quad u = v = T_y = 0, \tag{2.12a}$$

$$y = h(x): \quad v = u h_x, \tag{2.12b}$$

$$-p + 2N^{-2}[h_x^2 u_x + v_y - h_x(v_x + u_y)] = Ca^{-1} N^{-3} h_{xx}(1 - Ca\, T), \tag{2.12c}$$

$$2h_x(-u_x + v_y) + (1 - h_x^2)(v_x + u_y) = -(T_x + h_x T_y) N, \tag{2.12d}$$

$$N^{-1}(-h_x T_x + T_y) + Bi(T - T_g) = 0, \tag{2.12e}$$

where (2.12*b*) is the kinematic condition, (2.12*c*) and (2.12*d*) are the stress balances in the normal and tangential directions, respectively, and (2.12*e*) describes the heat transfer condition. In (2.12*c*) Ca is the capillary number, given by

$$Ca = \mu u_*/\sigma_* = \gamma(T_{max} - T_{min})/\sigma_*. \tag{2.13}$$

The Biot number Bi in (2.12*e*) is defined by

$$Bi = Hl/k \tag{2.14}$$

and measures the heat transport between the gas and the liquid phases.

3. Small-deformation theory

It is useful to begin this section with a short discussion of the known solutions of the equations given in §2. There is an exact solution

$$u = Cy, \quad v \equiv 0, \quad p \equiv 0, \quad T = -Cx + f(y), \quad h \equiv 1, \tag{3.1}$$

where $C = \text{const}$, which corresponds to plane Couette flow. Since there is a net mass flux in the x-direction, this solution is relevant only for infinite layers and it does not approximate flow in very long cavities. Birikh (1966) simulated the presence of the endwalls by enforcing zero mass flux across vertical sections and found, ignoring surface deflections, that $p \sim x$, $v = 0$ and u is given by Couette–Poiseuille flow. Sen & Davis (1982) considered asymptotically long cavities subject to linear heating and concluded that surface deflections remain small in the case of conduction-dominated Stokes flow provided that $CaL^4 = O(1)$, where L is the length of the cavity. Sen (1986) extended this analysis to the case of $CaL^3 = O(1)$ and showed that large deformations may occur. Tan, Bankoff & Davis (1990) considered periodic heating in the small-wavenumber limit and, using assumptions similar to those used by Sen & Davis (1982), showed that the interface may become significantly distorted. Floryan & Krol (1991) considered conduction-dominated Stokes flow in three-dimensional layers and derived conditions under which the interface may undergo only small deformations.

In the following subsection, we shall explore the behaviour of non-isothermal liquid layers subject to arbitrary heating under the assumption that only small interfacial distortions may occur. We shall determine *a posteriori* conditions under which such an assumption is valid.

3.1. *Construction of a solution in the limit* $Ca \to 0$

The limit of small capillary number $Ca \to 0$ corresponds to the case of the mean surface tension being very large compared to the amplitude of its thermal variations. In such a situation, the shape of the interface is expected to be dominated by the (static) capillary forces, with the (dynamic) thermocapillary effect producing only small distortions. This situation occurs either in the case of liquids that display weak variations of surface tension with temperature (a common situation), or in the case of liquids subject to small temperature gradients along the interface.

Following Rybicki & Floryan (1987), we seek a solution in the form of asymptotic expansions

$$q = q_0 + Ca\,q_1 + O(Ca^2), \quad p = Ca^{-1}p_s + p_0 + Ca\,p_1 + O(Ca^2), \tag{3.2}$$

where q stands for each of u, v, T, h, D and V. The first term in the pressure expansion corresponds to the static pressure caused by the mean surface tension and its magnitude expresses the fact that it scales on the capillary (σ_*/l) rather than the dynamic

($\mu u_*/l$) pressure scale. The regular character of these expansions is confirmed by numerical experiments discussed in §4.

Substitution of expansion (3.2) into the field equations (2.10) and boundary conditions (2.12) and grouping of the terms of the same order of magnitude in Ca leads to a sequence of simplified problems. Only the leading-order equations are given below.

Problem O (Ca^{-1}):
$$p_{sx} = p_{sy} = 0; \tag{3.3a}$$
boundary condition:
$$-p_s = h_{0xx}(1+h_{0x}^2)^{-3/2}; \tag{3.3b}$$
volume constraint: volume is known (3.3c)

interface condition: $h_0 < D_0$ or $h_{0x} \to 0$ as $x \to \pm\infty$. (3.3d)

Problem O (Ca^0):
$$L_1(u_0, v_0) = 0, \quad L_2(u_0, v_0, p_0) = 0, \quad L_3(u_0, v_0, T_0) = 0: \tag{3.4a–c}$$
boundary conditions
$$y = 0: \quad u_0 = v_0 = T_{0y} = 0, \tag{3.5a}$$
$$y = h_0(x): \quad v_0 = u_0 h_{0x}, \tag{3.5b}$$
$$-p_0 + 2(1+h_{0x}^2)^{-1}[h_{0x}^2 u_{0x} + v_{0y} - h_{0x}(v_{0x} + u_{0y})] = \{h_{1xx} - h_{0xx}[T_0 + 3(1+h_{0x}^2)^{-1} h_{0x} h_{1x}]\}(1+h_{0x}^2)^{-3/2}, \tag{3.5c}$$
$$2h_{0x}(-u_{0x} + v_{0y}) + (1-h_{0x}^2)(v_{0x} + u_{0y}) = -(T_{0x} + h_{0x} T_{0y})(1+h_{0x}^2)^{1/2}, \tag{3.5d}$$
$$(1+h_{0x})^{-1/2}(-h_{0x} T_{0x} + T_{0y}) + Bi(T_0 - T_g) = 0; \tag{3.5e}$$
volume constraint:
$$\int_{-\infty}^{\infty} h_1 \, dx = 0: \tag{3.5f}$$
interface condition: $h_1 < D_1$ or $h_{1x} \to 0$ as $x \to \pm\infty$. (3.5g)

Equations (3.3) describe interface in the state of static equilibrium, with (3.3*b*) (the Young–Laplace equation) describing its shape under isothermal conditions. Equations (3.4) with boundary conditions (3.5*a*, *b*, *d*, *e*) describe thermocapillary convection. The normal stress boundary condition (3.5*c*) together with the constraints (3.5*f*, *g*) define the deformation problem describing changes $h_1(x)$ in the shape of the interface induced by the thermocapillary effect.

The solution procedure begins with the determination of the initial (isothermal) shape of the interface, followed by solution of the convection problem (with fixed interface), and concludes with the determination of the (small) interface deformation.

The validity of expansions (3.2) is subject to some restrictions. Scaling introduced in §2 assumes that the interface changes on the same lengthscale l as the temperature and velocity fields. The shape of the interface, however, results from the global rather than just local equilibrium conditions, as best exemplified by the volume constraint (2.5). Thus, some other lengthscale may be present in the problem and this scale may or may not be directly related to the character of the temperature field. Rescaling of h_x and h_{xx} on the right-hand side of (2.12*c*) with a new distinct lengthscale L leads to
$$\text{RHS} = Ca^{-1}(1+A^2 h_{\bar{x}}^2)^{1/2} A^2 h_{\bar{x}\bar{x}}(1 - Ca\,T), \tag{3.6}$$
where $A = l/L$ and $\bar{x} = Ax$. If L becomes very large, $A \to 0$ and expansions (3.2) become invalid. Since the upper bound on L is established by the geometrical constraints (i.e. by the total length of the interface), L may assume an arbitrarily large value in the case of an infinitely long layer. This may lead to the appearance of large interfacial distortions and breakdown of expansions (3.2). It will be shown in §4 that

these large distortions can actually occur and that they do result in the breakup of the layer. The question arises then whether it is possible to maintain a long continuous non-isothermal liquid layer. In §3.2, we shall derive explicit conditions for the type of external heating applied to the interface that guarantees the existence of such layer. Such heating cannot give rise to a too long lengthscale L in the deformation pattern. An obvious example is provided by a periodic heating with a not too long wavelength. In the case of localized heating, the form of the heating that does not lead to break up of the layer is not apparent. We shall demonstrate in §4 that external heating that does not satisfy the existence conditions does result in large interface distortions.

The magnitude of the interfacial distortion depends on the magnitude of the capillary number, as expressed by expansions (3.2). These expansions are valid for small but finite Ca. In the infinite-layer case, appearance of an arbitrarily large L is possible and thus large distortions may occur regardless of how small Ca is. It is then a rule rather than an exception that expansions of the type (3.2) are not valid, unless some other conditions explicitly preventing appearance of a too large L are imposed. In the finite-layer case, the maximum possible value of L is limited by the length of the layer. Thus, it is always possible to find a sufficiently small Ca to prevent the appearance of large distortion for a given length of the layer. In such cases expansions of the type (3.2) are generally valid.

Expansions similar to (3.2) had been frequently used in the literature in constructing solutions describing flow in long cavities (small-aspect-ratio limit), see Sen & Davis (1982). In the limit, as the length of the cavity is increased, the capillary number is assumed to decrease at a sufficiently rapid rate to guarantee fulfilment of all the constraints and boundary conditions. This type of limit can be realized experimentally by reducing the temperature gradient along the interface when $L \to \infty$. If the cavity is heated in the same manner while its length increases, large deformations and breakup of the layer would occur when the cavity becomes sufficiently long. Such an experiment is simulated in §4.

In the following subsection, we shall focus our attention on a layer of constant thickness, i.e.

$$h_0 = 1, \quad p_s = 0. \tag{3.7}$$

It can be shown that this layer is statically stable.

3.2. *Interface deformation*

The deformation equation (3.5*c*) and the constraint conditions (3.5*f*, *g*) reduce in the case of a plane layer to the following form:

$$h_{1xx} = W(x), \qquad \int_{-\infty}^{\infty} h_1 \, dx = 0, \tag{3.8a, b}$$

$$h_1 < D_1 \quad \text{or} \quad h_{1x} \to 0 \quad \text{as} \quad x \to \pm\infty, \tag{3.8c, d}$$

where

$$W(x) = -\bar{p}_0(x, 1) + 2v_{0y}(x, 1) - B \tag{3.8e}$$

is referred to as the loading function, $\bar{p}_0$ denotes pressure normalized in an arbitrary way and B stands for the corresponding normalization constant. It should be stressed that (3.8) remains valid for arbitrary values of Re and Ma, as long as the interface distortion remains small.

We shall focus the following discussion on the case of an interface being flat as $x \to \pm\infty$, i.e. being subject to boundary conditions (3.8*d*). The existence and character of solutions of (3.8*a*, *b*, *d*) depend on the behaviour of the loading function $W(x)$ in the

limits $x \to \pm\infty$. The obvious condition is that $W(x) \to 0$ as $x \to \pm\infty$. Simple integration of (3.8*a*) and application of boundary conditions (3.8*d*) gives

$$\int_{-\infty}^{\infty} W(x)\,\mathrm{d}x = 0, \tag{3.9}$$

which is the necessary condition for existence of a solution of the deformation problem. If we further assume that $W(x)$ is absolutely convergent for $x \to \pm\infty$, then double integration of (3.8*a*) followed by integration by parts and imposition of (3.8*b*) and (3.8*d*) gives a deformation in the form

$$h_1(x) = x\int_{-\infty}^{x} W(\xi)\,\mathrm{d}\xi - \int_{-\infty}^{x} \xi W(\xi)\,\mathrm{d}\xi + \tfrac{1}{2}\int_{-\infty}^{\infty} \xi W(\xi)\,\mathrm{d}\xi \tag{3.10}$$

provided that

$$\int_{-\infty}^{\infty} xW(x)\,\mathrm{d}x = G, \qquad \int_{-\infty}^{\infty} x^2 W(x)\,\mathrm{d}x = 0, \tag{3.11\,a, b}$$

$$|W(x)| = o(|x|^{-3}) \quad \text{as} \quad x \to \pm\infty, \tag{3.11\,c}$$

where $G = O(1)$ is a constant. Equations (3.11) define sufficient conditions for the existence of solutions. It is possible that conditions (3.11) may not be satisfied while the solution of the deformation problem exists as, for example, is the case when $W(x)$ decays in an oscillatory manner but at a less rapid rate than required by (3.11*c*). An example of such a loading function is given in Appendix A. In the case of a localized heating, dynamical effects far away from the heat source decay exponentially with distance and thus (3.11*c*) is satisfied automatically while (3.11*a*, *b*) assume the role of the necessary conditions. This is the case of most interest in practical applications.

One may note that

$$h_1 \to \tfrac{1}{2}G \quad \text{as} \quad x \to -\infty; \qquad h_1 \to -\tfrac{1}{2}G \quad \text{as} \quad x \to +\infty,$$

and thus, if we want the layer to be unaffected by heating at $x \to \pm\infty$, the loading function $W(x)$ must satisfy (3.11*a*) with $G = 0$.

An interesting example that demonstrates the generality of the existence conditions is provided by the special solution (3.1) which is valid for arbitrary *Ca*. In this case $W(x) \equiv 0$ the existence conditions (3.9) and (3.11) are satisfied, the surface deformation becomes $h_1(x) \equiv 0$ and the asymptotic series (3.2) collapse to the leading term only.

Conditions (3.9) and (3.11) define the type of external heating applied to the interface that guarantees the existence of small deformations only. In general, these conditions can be tested only *a posteriori*, since the relation between the external heating and the function W is not explicit. In the special case of $Re = Ma = 0$, this relation can be determined using Fourier transforms (see Appendix B). This case will now be discussed in detail.

Fourier transform $\hat{W}(k)$ of $W(x)$ is defined (following (B 3)) as

$$\hat{W}(k) = (2\pi)^{-1/2}\int_{-\infty}^{\infty} W(x)\,\mathrm{e}^{\mathrm{i}kx}\,\mathrm{d}x. \tag{3.12}$$

Since we assume the existence of a Fourier transform of W and its derivatives, condition (3.11*c*) is satisfied and (3.11*a*, *b*) become the necessary conditions. All the existence conditions (3.9), (3.11*a*, *b*) can be expressed as

$$\hat{W}(0) = 0, \quad \frac{\mathrm{d}\hat{W}(0)}{\mathrm{d}k} = \mathrm{i}G(2\pi)^{-1/2}, \quad \frac{\mathrm{d}^2\hat{W}(0)}{\mathrm{d}k^2} = 0, \tag{3.13}$$

where i denotes imaginary unit. $\hat{W}(k)$ can be evaluated from solution (B 4), i.e.

$$\hat{W}(k) = \frac{Bi\cosh(k)}{k\sinh(k)+Bi\cosh(k)}\frac{2k^3}{\sinh(2k)-2k}\hat{T}_g(k), \tag{3.14}$$

where $\hat{T}_g(k)$ stands for the Fourier transform of the temperature $T_g(x)$ of the gas phase. Equations (3.13) require that

$$\hat{T}_g(0) = 0, \quad \frac{3}{2}\frac{d\hat{T}_g(0)}{dk} = iG(2\pi)^{-1/2}, \quad \frac{d^2\hat{T}_g(0)}{dk^2} = 0, \tag{3.15}$$

which, in view of the definition of the Fourier transform, requires that the external temperature field satisfies the following conditions

$$\int_{-\infty}^{\infty} T_g(x)\,dx = 0, \quad \int_{-\infty}^{\infty} xT_g(x)\,dx = \tfrac{2}{3}G, \quad \int_{-\infty}^{\infty} x^2T_g(x)\,dx = 0. \tag{3.16a–c}$$

Equations (3.16) give explicit form of the existence conditions in the case of $Re = Ma = 0$. The same form of conditions is also valid for $Bi = \infty$, $Re = 0$ and arbitrary Ma. A two-dimensional version of conditions (3.16) for the case of an interface being unaffected by the heating far away from the heating area was given by Floryan & Krol (1991).

We shall now focus our discussion on the interface subject to small (and finite) deformation for $x \to \pm\infty$, i.e. described by boundary condition (3.8*c*). We shall consider only one class of solutions, i.e. those corresponding to a periodic heating. Double integration of (3.8*a*) over a single period followed by integration by parts and imposition of a periodicity condition on W, h_1, and h_{1x} together with the volume constraint (3.8*b*) result in the deformation in the form

$$h_1(x) = x\int_0^x W(\xi)\,d\xi - \int_0^x \xi W(\xi)\,d\xi + \left(\frac{x}{L_p}+\frac{1}{2}\right)\int_0^{L_p}\xi W(\xi)\,d\xi - \frac{1}{2L_p}\int_0^{L_p}\xi^2 W(\xi)\,d\xi, \tag{3.17}$$

where L_p denotes the length of the period. In the special case of $Re = Ma = 0$ and $T_g(x) = T_a\sin(\alpha x)$ (see Appendix B, (B 5)) the deformation becomes

$$h_1(x) = -\frac{T_a Bi\cosh(\alpha)}{\alpha\sinh(\alpha)+Bi\cosh(\alpha)}\frac{2\alpha}{\sinh(2\alpha)-2\alpha}\sin(\alpha x). \tag{3.18}$$

For a very long wavelength of heating ($\alpha \to 0$), the amplitude of the deformation increases without bounds, i.e.

$$h_1(x) \to -\tfrac{3}{2}T_a\alpha^{-2}\sin(\alpha x) \quad \text{as} \quad \alpha \to 0. \tag{3.19}$$

Equation (3.19) shows that large interface deformation may occur even in the case of periodic heating provided that the wavelength of the heating is sufficiently long. This is in agreement with predictions of Tan *et al.* (1990).

4. Direct solution

In this section, we shall discuss the behaviour of the liquid layer subject to various types of external heating that could be of interest in practical applications. Conditions (3.11*a–c*) become necessary in such circumstances. We shall demonstrate that the response of the layer consists primarily of large interfacial distortion (and breakup), unless existence conditions (3.9), (3.11*a–c*) are strictly enforced. Since the non-

isothermal layer cannot exist when the external heating does not satisfy the above conditions, we shall consider flow in a finite cavity, as shown in figure 2, and observe the pattern of the interface deformation as the length L of the cavity increases. We shall demonstrate that conditions (3.9), (3.11*a–c*), which are strictly speaking valid only for infinite layers, also give a good indication of the behaviour of finite layers, i.e. the lack of existence of non-isothermal layers is not an artifact of the infinite-length assumption but a characteristic feature of this class of problems. We shall carry out numerical solution of the complete moving-boundary problem (2.10) with the complete boundary conditions (2.12) in order to determine the actual behaviour of the liquid without any assumptions that might be interpreted as being too restrictive. This approach permits demonstration of the generality of the existence conditions (3.9), (3.11*a–c*).

Motion of the liquid inside the cavity shown in figure 2 is governed by (2.10) with the boundary conditions at the bottom of the cavity given by (2.12*a*) and at the interface by (2.12*b–e*). Boundary conditions at the sidewall are given as

$$x = -\tfrac{1}{2}L: \quad u = v = 0, \quad T = T_L; \tag{4.1a}$$

$$x = \tfrac{1}{2}L: \quad u = v = 0, \quad T = T_R. \tag{4.1b}$$

Thermal conditions in (4.1) and temperature distribution in the gas phase $T_g(x)$ in (2.12*e*) must satisfy consistence conditions at the upper corners.

The type of contact between the interface and the sidewalls that corresponds to (2.6*b*) is

$$h_x = 0 \quad \text{at} \quad x = \pm\tfrac{1}{2}L. \tag{4.2a}$$

The above condition describes an interface which is allowed to move along the sidewalls with the constant contact angle fixed at 90°. We shall also consider a more constraining condition of fixed contact points, i.e.

$$h = 1 \quad \text{at} \quad x = \pm\tfrac{1}{2}L. \tag{4.2b}$$

One should keep in mind that in this case the existence conditions become more restrictive, i.e. $G = 0$ in (3.11*a*).

In the present case, the volumetric constraint condition assumes the form

$$\int_{-L/2}^{L/2} h \, \mathrm{d}x = V. \tag{4.3}$$

4.1. *Numerical algorithm*

A detailed description of the algorithm and testing of its accuracy were presented by Chen & Floryan (1994). The following description is limited to a short outline.

The governing equations are expressed in terms of a streamfunction (ψ) – vorticity (ω) formulation and are transformed from the irregular physical domain (defined by $h(x)$) in the (x, y)-plane into a rectangular computational domain in the (ξ, η)-plane (figure 2). The equations assume the following form:

$$\nabla^2\psi = -\omega, \tag{4.4a}$$

$$\nabla^2\omega = Re\, h^{-1}(\psi_\eta \omega_\xi - \psi_\xi \omega_\eta), \tag{4.4b}$$

$$\nabla^2 T = Ma\, h^{-1}(\psi_\eta T_\xi - \psi_\xi T_\eta), \tag{4.4c}$$

where

$$\left.\begin{gathered} x = \xi, \quad \eta = y/h(x), \quad u = \psi_y, \quad v = -\psi_x, \quad \omega = -u_y + v_x \\ \nabla^2 = \frac{\partial^2}{\partial\xi^2} - 2\eta h_\xi h^{-1}\frac{\partial^2}{\partial\xi\,\partial\eta} + (\eta^2 h_\xi^2 + 1)\,h^{-2}\frac{\partial^2}{\partial\eta^2} + (2h_\xi^2 - hh_{\xi\xi})\,\eta h^{-2}\frac{\partial}{\partial\eta}. \end{gathered}\right\} \tag{4.4d}$$

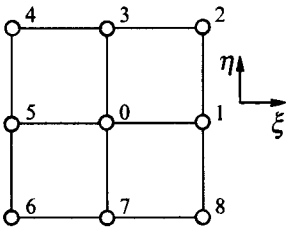

FIGURE 3. Sketch of a typical computational molecule.

The boundary conditions transform to

$$\xi = -\tfrac{1}{2}L: \quad \psi = \psi_\xi = 0, \quad T = T_L, \tag{4.5a}$$

$$\xi = \tfrac{1}{2}L: \quad \psi = \psi_\xi = 0, \quad T = T_R, \tag{4.5b}$$

$$\eta = 0: \quad \psi = \psi_\eta = 0, \quad T_\eta = 0, \tag{4.5c}$$

$$\eta = 1: \quad \psi = 0, \tag{4.5d}$$

$$p - 2(1+h_\xi^2)^{-1}[-(1+h_\xi^2)h^{-1}\psi_{\xi\eta} + h_\xi h^{-2}(h_\xi^2 - h_{\xi\xi}h + 1)\psi_\eta] + Ca^{-1}h_{\xi\xi}(1 - Ca\,T)(1+h_\xi^2)^{-3/2} = 0, \tag{4.5e}$$

$$(1+h_\xi^2)^2 h^{-2}\psi_{\eta\eta} - 2h_\xi(1+h_\xi^2)h^{-1}\psi_{\xi\eta} + [(1-h_\xi^2)hh_{\xi\xi} + (1+h_\xi^2)2h_\xi^2]h^{-2}\psi_\eta = -(1+h_\xi^2)^{1/2}T_\xi, \tag{4.5f}$$

$$(1+h_\xi^2)^{1/2}h^{-1}T_\eta - h_\xi(1+h_\xi^2)^{-1/2}T_\xi + Bi(T - T_g) = 0. \tag{4.5g}$$

The forms of the contact conditions and the volumetric constraint condition remain unchanged.

The above equations are solved using Picard-type iteration on the shape of the interface. An initial estimate of the shape of the interface is made, then the flow problem is solved with the assumed form of the interface without enforcing the normal stress boundary condition, and finally, the normal stress boundary condition is used to test whether the initial approximation of the interface was accurate. This procedure is repeated until a sufficiently accurate estimate of the location of the interface is obtained. The algorithm easily deals with the case of small-deformation theory described in §3, where it terminates after one complete cycle.

A finite-difference discretization procedure is used. A rectangular computational grid of size $\Delta\xi$, $\Delta\eta$ in the ξ, η directions is utilized, with grid lines parallel to the ξ- and η-axes and such that the grid fits exactly the geometry of the computational domain, with the side and bottom walls and the interface as certain grid lines. Around a typical interior grid point (ξ_0, η_0) we adopt the convention that quantities at (ξ_0, η_0) and in eight neighbouring points are denoted by subscripts 0, 1, ..., 8, as shown in figure 3. Then (4.4*a*, *b*) are approximated by using central second-order differences in the usual manner, to give

$$-2(A_1+A_2)\psi_0 + A_1\psi_1 - A_3\psi_2 + (A_2+A_4)\psi_3 + A_3\psi_4 + A_1\psi_5 - A_3\psi_6 + (A_2-A_4)\psi_7 + A_3\psi_8 + \omega_0 = 0, \tag{4.6a}$$

$$-2(A_1+A_2)\omega_0 + [A_1 - Re\,A_5(\psi_3 - \psi_7)]\omega_1 - A_3\omega_2 + [A_2 + A_4 + Re\,A_5(\psi_1 - \psi_5)]\omega_3 + A_3\omega_4 + [A_1 + Re\,A_5(\psi_3 - \psi_7)]\omega_5 - A_3\omega_6 + [A_2 - A_4 - Re\,A_5(\psi_1 - \psi_5)]\omega_7 + A_3\omega_8 = 0, \tag{4.6b}$$

where

$$A_1 = \Delta\xi^{-2}, \quad A_2 = (1+\eta^2 h_\xi^2)(h\Delta\eta)^{-2}, \quad A_3 = \eta h_\xi(2h\Delta\xi\Delta\eta)^{-1},$$
$$A_4 = \eta(2h_\xi^2 - hh_{\xi\xi})(2h^2\Delta\eta)^{-1}, \quad A_5 = (4h\Delta\xi\Delta\eta)^{-1}.$$

The discretized energy equation has the same form as (4.6*b*) with ω replaced by T and Re replaced by Ma.

The boundary conditions for (4.6) are given by (4.5*a–d, f, g*). For (4.6*a*), values of ψ are known at all grid points on the solid walls and along the interface. For (4.6*b*), a boundary condition for ω is required at grid points on the solid walls. It follows from (4.4*a*) and (4.5*a, b*) that at the sidewalls $\omega = -\psi_{\xi\xi}$, which, after a second-order approximation, assumes the form

$$\omega_b = (\psi_{i+1} - 8\psi_i)/2\Delta^2, \tag{4.7a}$$

where subscript b refers to the wall values, subscript i refers to the internal grid point most immediate to b, subscript $i+1$ refers to the next grid point in the same direction and Δ denotes grid size. At the bottom, $\omega = -\psi_{\eta\eta} h^{-2}$ and the boundary condition for vorticity becomes

$$\omega_b = (\psi_{i+1} - 8\psi_i)/2\Delta^2 h^2. \tag{4.7b}$$

The boundary condition at the interface is obtained by substituting (4.5*f*) into (4.4*a*) resulting in

$$\omega = \frac{(1+h_\xi^2)^{1/2} T_\xi h + 2h_{\xi\xi}\psi_\eta}{h(1+h_\xi^2)}. \tag{4.7c}$$

In the above, T_ξ is evaluated using a standard central-difference approximation, and ψ_η is determined using a one-sided difference approximation. Both T_ξ and ψ_η have to be updated during the iteration process. For the energy equation, values of T are known at the sidewalls. At the remaining two boundaries T is determined from the discretized boundary conditions (4.5*c*) and (4.5*g*). All discretization formulae are second-order accurate.

The discretized field equations were solved by the standard Gauss–Seidel relaxation procedure. The systematic iterative procedure between the various equations consisted of performing one complete Gauss–Seidel iteration of (4.6*a*), followed by similar iteration of (4.6*b*) and then a complete iteration of the energy equation followed by a recalculation of the boundary values of ω and T. The iteration was performed until the convergence criteria

$$|\omega^{(i+1)} - \omega^{(i)}| < \epsilon, \quad |\psi^{(i+1)} - \psi^{(i)}| < \epsilon, \quad |T^{(i+1)} - T^{(i)}| < \epsilon, \quad |\mathrm{Res}_1^{(i)}| < \epsilon,$$
$$|\mathrm{Res}_2^{(i)}| < \epsilon, \quad |\mathrm{Res}_3^{(i)}| < \epsilon$$

with $\epsilon = 10^{-6}$ and i denoting the iteration number, were satisfied at all grid points. In the above, Res_1, Res_2 and Res_3, stand for the residua of the discretized equations (4.4*a*), (4.4*b*), and (4.4*c*), respectively. Those criteria were judged to be generally satisfactory; nevertheless certain cases were additionally checked by reducing the criterion to $\epsilon = 10^{-9}$. The relaxation factor used in the calculations varied from 1.0 for flat interface to 0.05 for very deformed interfaces. These factors had to be further reduced with increasing values of Re and Ma.

Equations (4.6) and (4.7) treat the location of the interface as being known, with h denoting its most recent (from the last Picard iteration) approximation. After ψ and ω had been determined with sufficient accuracy, a new shape of interface is found by solving the deformation problem consisting of (4.5*e*) and (4.3) and either (4.2*a*) or (4.2*b*).

Equation (4.5*e*) requires knowledge of pressure at the interface. Pressure is evaluated from the x-component of (2.10*b*) and the known solution of (4.4), e.g.

$$p_\xi = h_\xi \omega_\xi - (1+h_\xi^2) h^{-1}\omega_\eta - Re\, h^{-2}\psi_\eta[(1+h_\xi^2)\psi_{\xi\eta} + h_\xi h^{-1}(h_{\xi\xi}h - h_\xi^2 - 1)\psi_\eta]. \tag{4.8}$$

The above expression is integrated using the trapezoidal rule in the $\pm\xi$-directions beginning at $\xi = 0$. The calculated pressure is denoted by $\bar{p}$ to show that it is normalized with condition $\bar{p}(0, 1) = 0$. The mixed derivative of the streamfunction at the interface appearing in (4.8) is evaluated according to the formula

$$\psi_{\xi\eta} = [3(\psi_2 - \psi_4) - 4(\psi_1 - \psi_5) + \psi_8 - \psi_6]/4\,\Delta\xi\,\Delta\eta + O(\Delta\xi^2) + O(\Delta\eta^2), \tag{4.9}$$

where subscripts refer to the points shown schematically in figure 3, with the points 2, 3 and 4 located on the interface. Other mean flow quantities are evaluated using standard one-sided or central second-order finite-difference approximations.

Equations (4.5*e*) defines a two-point boundary-value problem for h subject to a constraint condition (4.3). In the numerical solution, (4.5*e*) and (4.3) are treated as a system of equations and are solved directly. The pressure and shape of the interface are represented as

$$p = Ca^{-1}p_s + \bar{p} + B, \quad h = h_0 + h_1, \quad p_s = -h_{0\xi\xi}(1 + h_{0\xi}^2)^{-3/2}, \tag{4.10a–c}$$

where h_0 denotes the known shape of the isothermal interface corresponding to the known volume of the liquid (4.3), p_s stands for the known pressure of the isothermal liquid, h_1 denotes the change of shape of the interface due to non-isothermal effects, $\bar{p}$ denotes pressure associated with the thermocapillary convection and determined numerically from the solution of the field equations (4.8) and B stands for an arbitrary constant than can be present in the pressure field. Pressure $\bar{p}$ satisfies the normalization condition $\bar{p}(0, 1) = 0$. Equation (4.5*e*) can be written, for any grid point along the interface, in the form

$$F_i(\hat{h}_i, \hat{h}_{\xi i}, \hat{h}_{\xi\xi i}, B) = 0, \tag{4.11}$$

where $\hat{h}_i$, $\hat{h}_{\xi i}$, $\hat{h}_{\xi\xi i}$, $i = 1, \ldots, N$, denote values of h_1, $h_{1\xi}$, $h_{1\xi\xi}$ at the grid points with $i = 1$ corresponding to the left contact point, and all the remaining quantities being known. Derivatives in (4.11) are approximated using standard central-difference approximations leading to an equation in the form

$$F_i(\hat{h}_{i-1}, \hat{h}_i, \hat{h}_{i+1}, B) = 0, \tag{4.12}$$

which is then linearized using the Newton–Raphson procedure

$$F_i(\hat{h}_{i-1}^{(k+1)}, \hat{h}_i^{(k+1)}, \hat{h}_{i+1}^{(k+1)}, B^{(k+1)}) = F_i(\hat{h}_{i-1}^{(k)}, \hat{h}_i^{(k)}, \hat{h}_{i+1}^{(k)}, B^{(k)}) + \frac{\partial F_i}{\partial \hat{h}_{i-1}}(\hat{h}_{i-1}^{(k+1)} - \hat{h}_{i-1}^{(k)}))$$

$$+ \frac{\partial F_i}{\partial \hat{h}_i}(\hat{h}_i^{(k+1)} - \hat{h}_i^{(k)}) + \frac{\partial F_i}{\partial \hat{h}_{i+1}}(\hat{h}_{i+1}^{(k+1)} - h_{i+1}^{(k)}) + (B^{(k+1)} - B^{(k)}) = 0. \tag{4.13}$$

In the above, superscripts denote iteration count and derivatives are evaluated analytically at $\hat{h}_{i-1}^{(k)}$, $\hat{h}_i^{(k)}$, $\hat{h}_{i+1}^{(k)}$. Now (4.13) can be rewritten as

$$A_i \hat{h}_{i-1}^{(k+1)} + B_i \hat{h}_i^{(k+1)} + C_i \hat{h}_{i+1}^{(k+1)} = M_i^{(k)}, \tag{4.14}$$

where

$$M_i^{(k)} = \frac{\partial F_i}{\partial \hat{h}_{i-1}} \hat{h}_{i-1}^{(k)} + \frac{\partial F_i}{\partial \hat{h}_i} \hat{h}_i^{(k)} + \frac{\partial F_i}{\partial \hat{h}_{i+1}} \hat{h}_{i+1}^{(k)} + B_{(k)} - F_i^{(k)} \quad \text{and} \quad \hat{h}_{i-1}^{(k)}, \hat{h}_i^{(k)}, \hat{h}_{i+1}^{(k)}$$

are known. Such an equation can be written for each grid point along the interface. The volume constraint condition (4.3), which takes the form

$$\int_{-L/2}^{L/2} h_1 \, \mathrm{d}x = 0, \tag{4.15}$$

	Temperature distribution $T(x)$	$\int_{-L/2}^{L/2} T(x)\,dx$	$\int_{-L/2}^{L/2} xT(x)\,dx$	$\int_{-L/2}^{L/2} x^2T(x)\,dx$
A	$-x/L$	0	$-L^2/12$	0
B	$-x$	0	$-L^3/12$	0
C	$10\,e^{-x^2}$	$10\pi^{1/2}\,\mathrm{erf}(L/2)$	0	$-5L\,e^{-L^2/4}$ $+5\pi^{1/2}\,\mathrm{erf}(L/2)$
D	$(4x^3-6x)\,e^{-x^2}$	0	$-L^3\,e^{-L^2/4}/2$	0
E	$(4x^3-6x)\,e^{-1.5x^2}$	0	$-0.96\,\mathrm{erf}(0.61L)$ $+0.67L\,e^{-0.375L^2}$ $-0.33L^3\,e^{-0.375L^2}$	0

(erf denotes the error function)

TABLE 1. External temperature fields subject to the investigations and their moments

is discretized using the trapezoidal rule and forms an algebraic equation involving $\hat{h}_i$ at all grid points. The system of equations consisting of (4.14) written for each grid point and (4.15) is closed by contact conditions (4.2*a*) or (4.2*b*). The resulting matrix equation is solved directly using an algorithm described by Chen & Floryan (1994).

The procedure described above for solution of the (nonlinear) deformation problem has a quadratic rate of convergence and 3–4 iterations to reduce the error to the machine accuracy level.

The efficiency of the whole algorithm strongly depends on the particular values of the parameters present in the problem, like *Re*, *Ma*, and *Ca*. The most efficient solution was obtained by carrying out one iteration on the flow field followed by one iteration of the interface. In all cases strong under-relaxation (0.01–0.1) was used when adjusting the shape of the interface. This under-relaxation increased with increasing values of *Ca*. Extensive testing showed that the algorithm delivers second-order accuracy as a function of grid size. See Chen & Floryan (1994) for further details.

4.2. *Deformation analysis*

We shall investigate the behaviour of the interface subject to the five types of external heating shown in table 1. In order to simplify the following discussion, we shall only consider the case $Re = Ma = 0$, $Bi = \infty$. This makes the temperature of the interface equal to the temperature of the gas phase $T_g(x)$. Also, the existence conditions (3.9), (3.11*a–c*) can be expressed explicitly in terms of the interface temperature, e.g. (3.16).

Temperature distribution A (table 1) describes a cavity whose ends are kept at constant (but different) temperatures. Conduction dominates in the gas phase leading to a linear temperature variation along the interface, which does not satisfy the existence conditions. The temperature gradient decreases as the length L of the cavity increases, leading to a weaker thermocapillary effect. This heating has frequently been studied before and is included in our analysis for comparison purposes. Sen & Davis (1982) treated a similar case but in the limit of $L \to \infty$ reduced the temperature difference between the endwalls proportionally to L^{-3}.

Temperature distribution B describes the situation where the temperature gradient along the interface is constant. This type of heating, which again does not satisfy the existence conditions, has been frequently studied in the literature (e.g. Birikh 1966).

Temperature distribution C has been selected in order to (qualitatively) represent temperature fields that can be found when the liquid is subject to heating using a localized heat source. This problem is of interest in various material processing

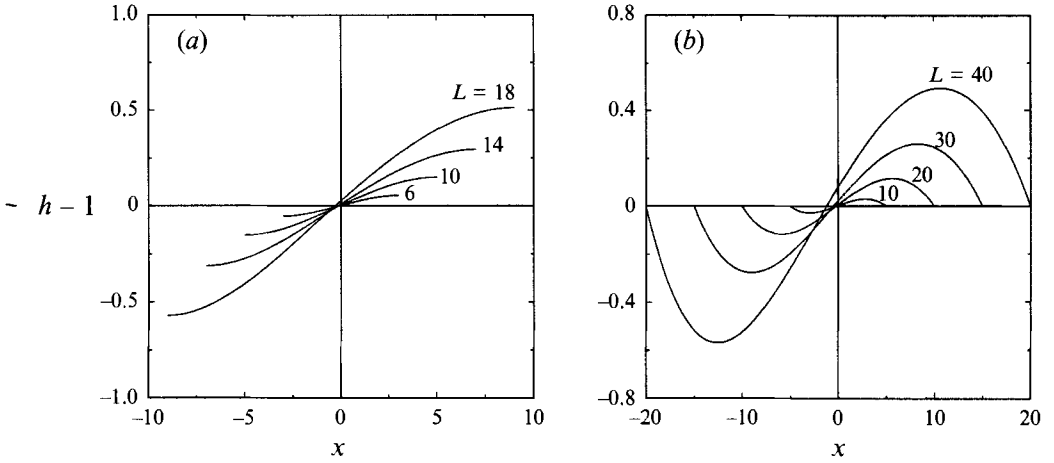

FIGURE 4. Interface deformation pattern. External heating of type A: $T_g(x) = -x/L$. $Re = Ma = 0$, $Bi = \infty$, $Ca = 0.024$. (*a*) Fixed contact angles ($\theta_L = \theta_R = 0$); (*b*) fixed contact points ($h(-\frac{1}{2}L) = h(\frac{1}{2}L) = 1$).

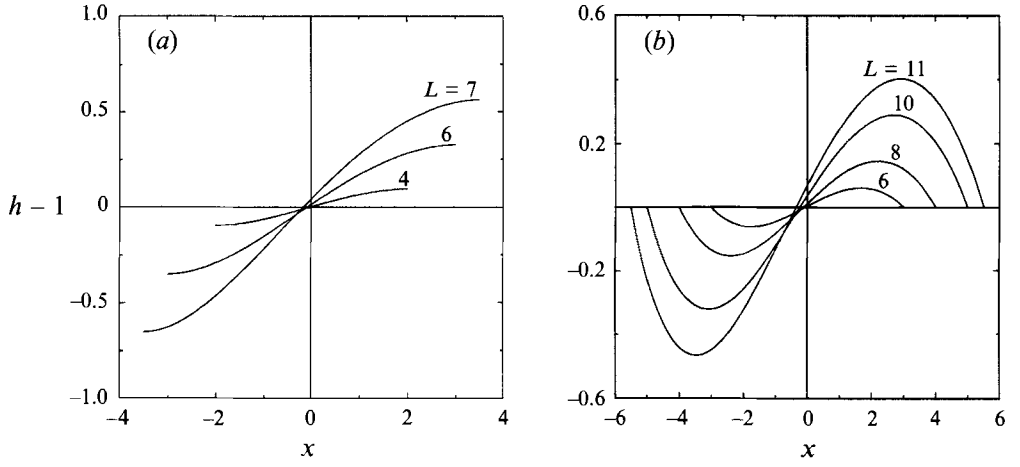

FIGURE 5. Interface deformation pattern. External heating of type B: $T_g(x) = -x$. (*a*) Fixed contact angles; (*b*) fixed contact points. All other conditions as in figure 4.

techniques. The corresponding temperature distribution does not satisfy the existence conditions. A possible lack of existence of a liquid layer subject to such a heating has been noted by Pimputkar & Ostrach (1980).

Temperature distribution D provides an example of heating that satisfies the existence condition with $G = 0$ in (3.16*b*). Temperature distribution E also satisfies the existence conditions, but with $G = -1.44$ in (3.16*b*).

Figures 4–8 display results of the direct numerical solution of the flow problems corresponding to the temperature distributions A–E, respectively. Calculations shown were obtained for $Ca = 0.024$ and for an interface that was initially flat (equation (3.7)). Results shown in figures 4(*a*), 5(*a*) and 6(*a*), which were obtained in the fixed-contact-angle case (4.2*a*), demonstrate that the temperature distributions A, B and C induce large distortions and lead to the breakup of the interface in a sufficiently long cavity. The character and details of the breakup process strongly depend on the

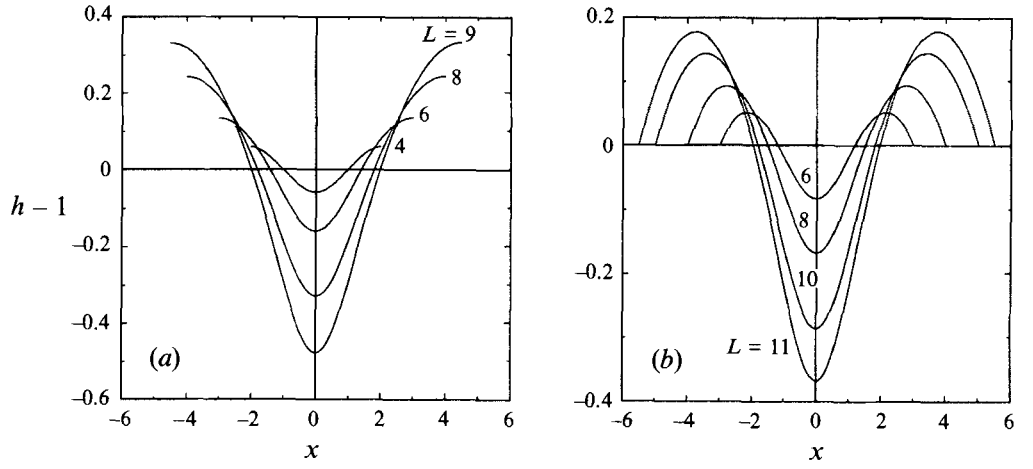

FIGURE 6. Interface deformation pattern. External heating of type C: $T_g(x) = 10\,e^{-x^2}$. (*a*) Fixed contact angles; (*b*) fixed contact points. All other conditions as in figure 4.

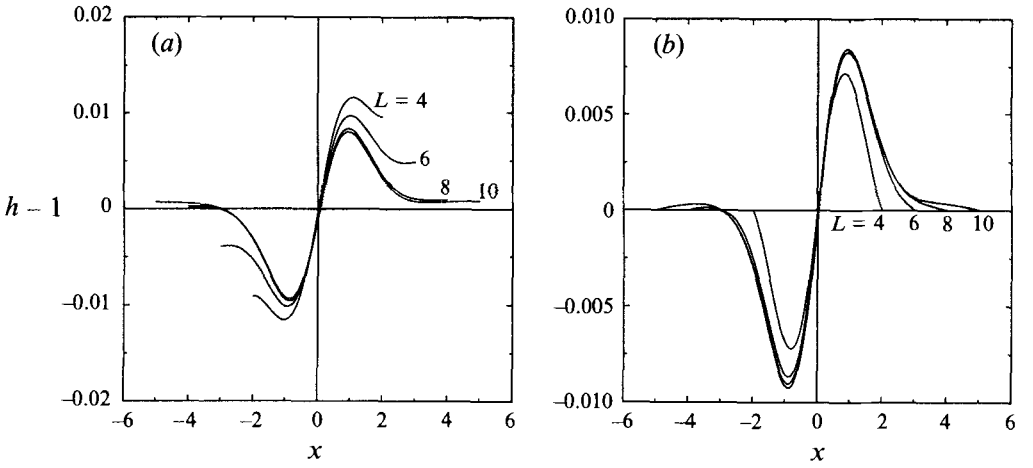

FIGURE 7. Interface deformation pattern. External heating of type D: $T_g(x) = (4x^3 - 6x)\,e^{-x^2}$. (*a*) Fixed contact angles; (*b*) fixed contact points. All other conditions as in figure 4.

functional form of the external heating. Fixing contact points, (4.2*b*), reduces the amplitude of the interface deformation but does not prevent breakup of the interface in a sufficiently long cavity, as shown in figures 4(*b*), 5(*b*), and 6(*b*). Temperature distributions D and E satisfy the existence condition and give rise only to small deformations, as shown in figures 7 and 8. In the following subsections, we shall discuss each case in detail.

4.2.1. *External heating in the form* $T(x) = -x/L$ *(Type A)*

Study of this type of heating was initiated by Sen & Davis (1982) in the case of very long cavities (cavity aspect ratio $L^{-1} \to 0$) and with the small-interface-deformation assumption. The problem is peculiar in the sense that in the limiting process (as the cavity becomes longer) the interface temperature gradient and thus the thermocapillary effect become smaller (and disappear in the limit). Sen & Davis (1982) demonstrated that the flow field may be divided into a core zone with Couette–Poiseuille flow (with

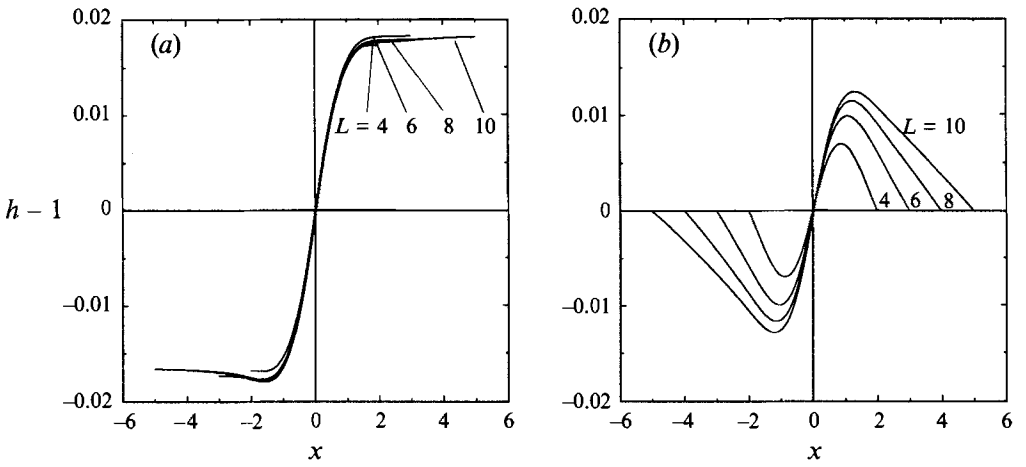

FIGURE 8. Interface deformation pattern. External heating of type E: $T_g(x) = (4x^3 - 6x)\,e^{-1.5x^2}$. (*a*) Fixed contact angles; (*b*) fixed contact points. All other conditions as in figure 4.

zero mass flux) and two turning zones, each at the opposite end of the cavity. Deformation of the interface is affected only by the core zone.

The flow in the core zone is driven by shear stress at the interface. There is a constant longitudinal pressure gradient required to generate backflow in order to conserve mass. While the pressure gradient becomes smaller in the limiting process, the total pressure variation from one end of the cavity to the other does not need to decrease, which is due to the increasing length of the cavity. It is simple to show that in the case of Couette–Poiseuille flow (with a flat interface)

$$u(y) = \frac{3}{4L}y^2 - \frac{1}{2L}y, \quad \frac{dp}{dx} = \frac{3}{2L}. \tag{4.16}$$

Solution of the (small) deformation problem (3.7) gives

$$h_1(x) = -\frac{x^3}{4L} + \frac{3Lx}{16}, \quad h_{1max} = h_1\left(\pm\frac{1}{2L}\right) = \frac{L^2}{16} \tag{4.17a, b}$$

in the fixed-contact-angle case and

$$h_1(x) = -\frac{x^3}{4L} + \frac{Lx}{16}, \quad h_{1max} = h_1\left(\frac{\pm L}{\sqrt{12}}\right) = \frac{L^2}{48 \times \sqrt{3}} \tag{4.18a, b}$$

in the fixed-contact-point case. Equations (4.16) shows that the total pressure variation remains the same as L increases, while the amplitude of deformation increases as L^2 ((4.17) and (4.18)) due to the increased distance between the contact points. One may note that (3.16*b*) predicts a similar rate of increase (see table 1 for the integral evaluation). The large deformation is eliminated in the solution of Sen & Davis (1982) by requiring that $Ca = O(L^{-3})$ when $L^{-1} \to 0$, which gives deformation in the form $h = 1 + Ca\,h_1 = 1 + L^{-1}\bar{h}_1$, where $\bar{h}_1 = O(1)$. Thus, they consider a limit of $L^{-1} \to 0$, $Ca \to 0$ but $L^4 Ca = O(1)$, which describes the case of the temperature difference between the endwalls decreasing at a rate of $O(L^{-3})$ as $L^{-1} \to 0$. Sen (1986) considered the case $Ca = O(L^{-2})$ and showed that deformations of $O(1)$ are possible. This requires reduction of temperature difference between the endwalls at the rate of $O(L^{-2})$. Both of the above solutions consider limits that require adjustment of external temperature.

(*a*)	$\lvert h(\frac{1}{2}L)-1\rvert$ (fixed contact angles) $Ca = 0.024$		
Cavity length L	Asymptotic solution ($Ca \to 0$) with the core flow approximation (Eqn (4.17*b*))	Asymptotic solution ($Ca \to 0$) with the complete flow field (Eqn (3.3))	Direct solution
6	0.054	0.0539	0.05385
10	0.15	0.1497	0.1527
14	0.294	0.2935	0.3112
18	0.486	0.4855	0.5714
19	0.5415	0.5412	0.6823
(*b*)	$\lvert h-1\rvert_{max}$ (fixed contact points) $Ca = 0.024$		
Cavity length L	Asymptotic solution ($Ca \to 0$) with the core flow approximation (Eqn (4.18*b*))	Asymptotic solution ($Ca \to 0$) with the complete flow field (Eqn (3.7))	Direct solution
6	0.0104	0.0101	0.01
10	0.0287	0.0287	0.0288
20	0.1155	0.115	0.1122
30	0.2598	0.2598	0.2769
40	0.4618	0.4618	0.5688

TABLE 2. Maximum interface deformation as a function of the cavity length. External heating of type A. $Re = Ma = 0$, $Bi = \infty$. (*a*) Fixed contact angles; (*b*) fixed contact points

If this temperature is fixed, these solutions describe liquid in a cavity that has to be long enough in order to develop the core zone in the flow field, but not too long in order to prevent appearance of large interfacial distortions. This 'window of opportunity' could be of practical value only for liquids with extremely small capillary number.

The evolution of the interface deformation as a function of the cavity length L is illustrated in table 2. The results show that the amplitude of deformation initially increases proportionally to L^2, and that the growth process is well approximated using the core-zone approximation of the flow field even for $h-1 = O(1)$, which confirms Sen's (1986) results. Comparison of tables 2(*a*) and 2(*b*) shows that while fixing of the location of the contact points strongly reduces the magnitude of the interface deformation, it does not affect qualitatively its rate of growth as a function of L.

4.2.2. *External heating in the form $T(x) = -x$ (type B)*

Study of this type of heating was initiated by Levich (1962) who analysed the flow in the central section of a long cavity. The interface was assumed to be flat and the flow was considered to be unaffected by the cavity ends and well approximated by the Couette–Poiseuille flow. Birikh (1966) generalized this solution without, however, addressing the issue of the interface deformation.

The structure of the flow field is similar to the one already discussed in §4.2.1. The only difference is that the strength of the thermocapillary effect remains the same as the length of the cavity increases. Not surprisingly, the breakup of the interface occurs for much shorter cavities, as illustrated in figure 5. Analysis similar to that leading to (4.16)–(4.18) results in

$$u(y) = \tfrac{3}{4}y^2 - \tfrac{1}{2}y, \quad \frac{dp}{dx} = \frac{3}{2} \tag{4.19}$$

(*a*)	$\lvert h(-\frac{1}{2}L)-1\rvert$ (fixed contact angles) $Ca = 0.024$		
Cavity length L	Asymptotic solution ($Ca \to 0$) with the core flow approximation (Eqn (4.20))	Asymptotic solution ($Ca \to 0$) with the complete flow field (Eqn (3.3))	Direct solution
4	0.096	0.096	0.0965
6	0.324	0.323	0.3504
7	0.515	0.5133	0.6516
7.1	0.5369	0.5354	0.7145
(*b*)	$\lvert h-1\rvert_{max}$ (fixed contact points) $Ca = 0.024$		
Cavity length L	Asymptotic solution ($Ca \to 0$) with the core flow approximation (Eqn (4.21))	Asymptotic solution ($Ca \to 0$) with the complete flow field (Eqn (3.3))	Direct solution
6	0.0624	0.0607	0.0622
8	0.148	0.146	0.153
10	0.287	0.287	0.322
11	0.384	0.383	0.466
11.5	0.439	0.4375	0.579

TABLE 3. Maximum interface deformation as a function of the cavity length. External heating of type B. $Re = Ma = 0$, $Bi = \infty$. (*a*) Fixed contact angles; (*b*) fixed contact points

and deformations in the fixed-contact-angle case in the form

$$h_1(x) = -\frac{x^3}{4} + \frac{3L^2x}{16}, \quad h_{1max} = h_1\left(\pm\frac{1}{2L}\right) = \frac{L^3}{16}, \tag{4.20a, b}$$

and in the fixed-contact-point case in the form

$$h_1(x) = -\frac{x^3}{4} + \frac{L^2x}{16}, \quad h_{1max} = h_1\left(\pm\frac{L}{\sqrt{12}}\right) = \frac{L^3}{48\times\sqrt{3}}. \tag{4.21a, b}$$

Equation (4.19) shows that the total pressure variations along the interface increase proportionally to L, while amplitude of the interface deformation increases as L^3 ((4.20) and (4.21)). Such growth is predicted by (3.16*b*) (see table 1 for value of the integral). Table 3 illustrates the evolution of the interface deformation as a function of L and confirms that this deformation grows initially proportionally to L^3 and that this growth is well approximated, even for fairly large deformations, by the core-zone approximation.

4.2.3. *External heating in the form* $T(x) = 10\,\mathrm{e}^{-x^2}$ *(type C)*

This particular temperature distribution has been selected in order to illustrate effects associated with heating of the liquid using a localized heat source. The existence conditions are not satisfied and the layer breaks up in a sufficiently long cavity, as illustrated by results shown in figure 6. We shall now explain the physical reasons for the breakup.

The liquid is driven by surface tension gradients along the interface away from the point of maximum temperature. The backflow along the bottom of the cavity is forced by the pressure rise on both sides of the heating area. Since the velocity magnitude decreases approximately exponentially with distance away from the heat source, this

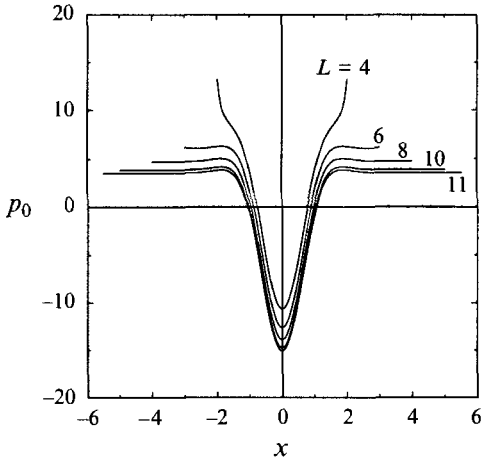

FIGURE 9. Interface pressure distribution $p_0(x, 1)$. Non-deformable interface. External heating of type C (see table 1). Fixed contact points. $Re = Ma = 0$, $Bi = \infty$.

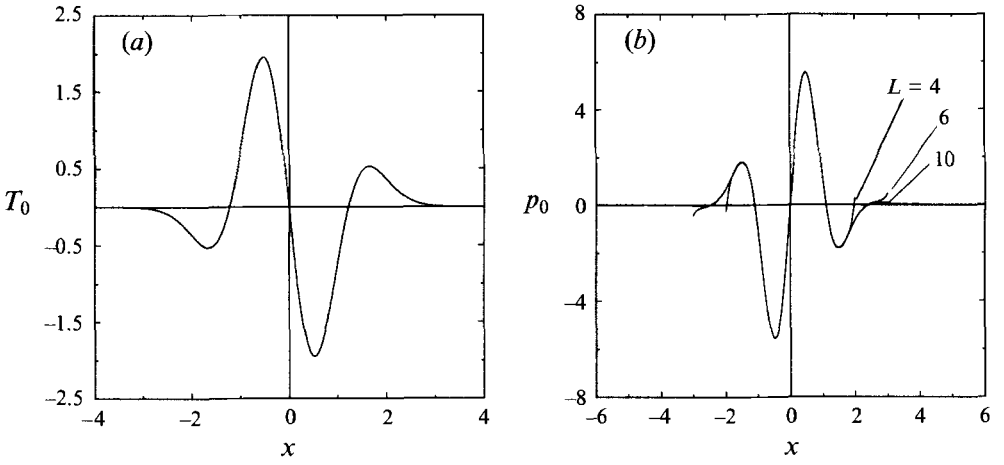

FIGURE 10. External heating of type D (see table 1). (*a*) Interface temperature distribution $T_0(x, 1)$; (*b*) surface pressure distribution $p_0(x, 1)$. Non-deformable interface. $Re = Ma = 0$, $Bi = \infty$.

pressure reaches a constant (non-zero) value sufficiently far away from the heat source, as illustrated in figure 9. This constant pressure would extend to the ends of the cavity regardless of the cavity length if the interface were non-deformable. In the case of a finite Ca, the constant pressure jump across the interface generates a large deformation regardless of the value of Ca, if the cavity is made sufficiently long. The deformation consists of outward bulging at both ends of the cavity (high-pressure areas) and inward bulging in the middle section (location of the heat source, low-pressure area), as shown in figure 6.

4.2.4. *External heating in the form* $T(x) = (4x^3 - 6x)\,e^{-x^2}$ *(type D)*

The functional form of this temperature distribution has been specially selected in order to satisfy the existence conditions. This heating is characterized by $G = 0$ in (3.16*b*). Its form is plotted in figure 10(*a*) and shows a pattern of localized heating and cooling. The resulting distribution of surface tension gradients is 'balanced' in the sense that it does not lead to any pressure changes far away from the heating area. Such

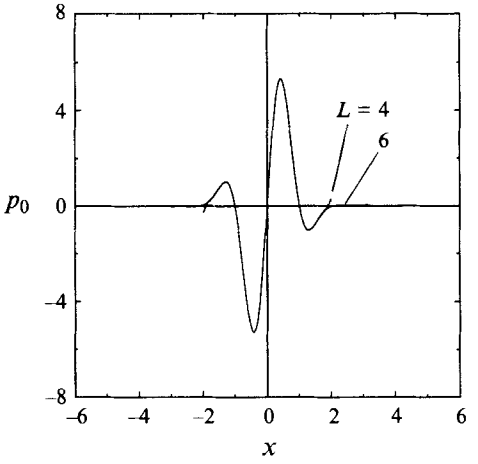

FIGURE 11. Interface pressure distribution $p_0(x, 1)$. Non-deformable interface. External heating of type E (see table 1). $Re = Ma = 0$, $Bi = \infty$.

changes were required in the case of heating discussed in the previous subsection in order to generate backflow. The pressure distribution is shown in figure 10(*b*). The resulting interface deformation, shown in figure 7, very rapidly approaches the form predicted for the infinite layer by (3.10), with $h_1(-\frac{1}{2}L)$, $h_1(\frac{1}{2}L) \to 0$ as $L \to \infty$.

4.2.5. *External heating in the form* $T(x) = (4x^3 - 6x)\,\mathrm{e}^{-1.5x^2}$ *(type E)*

This form of temperature distribution was selected specially in order to satisfy the existence conditions, but with $G \neq 0$ in (3.16*b*) ($G = -1.44$). The heating causes change of elevation of the interface at $x = \pm\infty$ and this is inconsistent in the limit of very long cavity $L \to \infty$ with the fixed-contact-point condition.

The physical situation is analogous to the one discussed in §4.2.4. The pressure distribution displayed in figure 11 shows that pressure levels off to zero with distance away from the heating area. The pattern of the interface deformation in the fixed-contact-angle case, which is shown in figure 8(*a*), demonstrates that the interface very rapidly reaches the form predicted for the infinite layer by (3.10), with $h_1(-\frac{1}{2}L) \to -0.72$ and $h_1(\frac{1}{2}L) \to 0.72$ as $L \to \infty$. The pattern of the deformation in the fixed-contact-point case is shown in figure 8(*b*), but it does not offer any insight into what happens as $L \to \infty$. One may recall that such a solution cannot exist for $L = \infty$. The maximum deformation increases as a function of L ($|h-1|_{max} = 0.0128, 0.0161, 0.018, 0.0195$ for $L = 10, 20, 30, 40$, respectively) which suggest possible occurrence of large deformations. The rate of increase is so small that it precludes detailed analysis of this phenomena using numerical simulation.

4.2.6. *Capillary number effects*

Figure 12(*a*) illustrates the evolution of the maximum interface deformation as a function of the capillary number Ca determined using asymptotic (equation (3.8)) and direct (§4.1) methods of solution. The displayed results have been obtained for external heating of type A and cavity length $L = 6$. These results demonstrate that for a cavity of a constant length the error of the asymptotic solution increases approximately proportionally to Ca^2, thus confirming the regular character of the expansions (3.2). Figure 12(*b*, *c*) shows the evolution of the pattern of the interface deformation. One may note that in the limiting case of $Ca \to 0$ (asymptotic solution), the deformation is

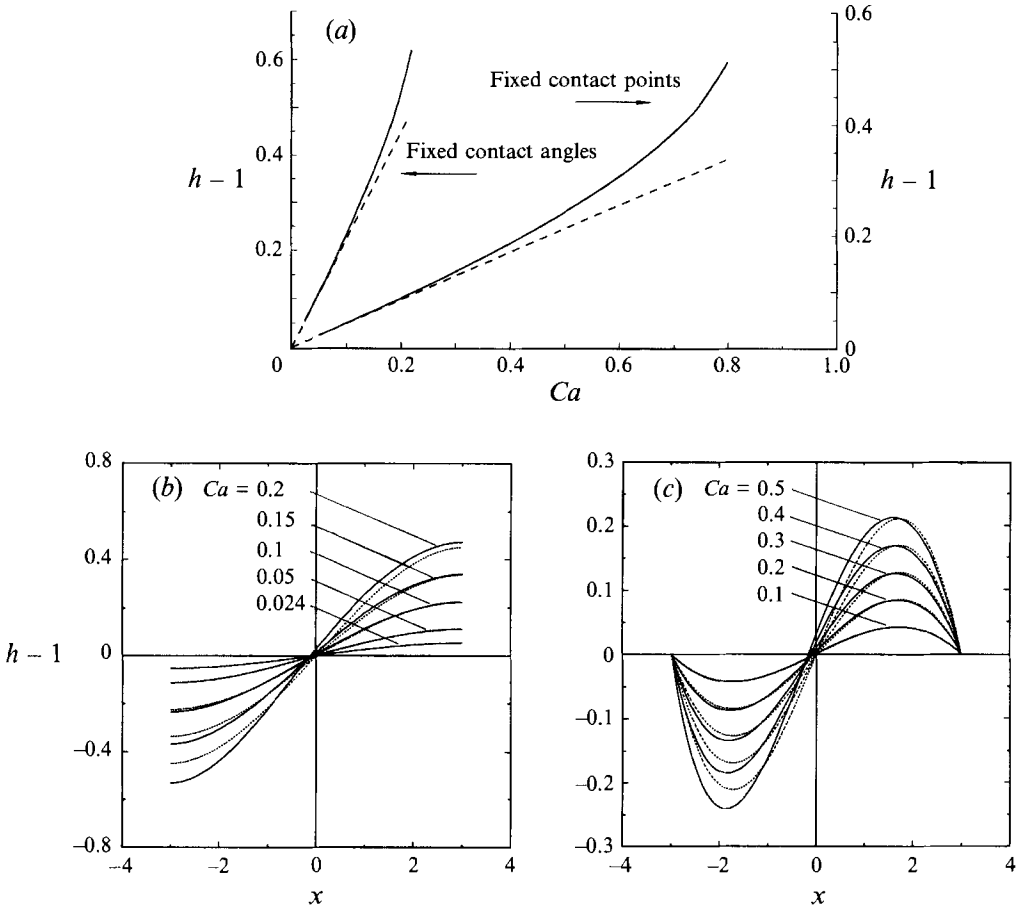

FIGURE 12. Interface deformation as a function of capillary number Ca. $Re = Ma = 0$, $Bi = \infty$, $L = 6$. External heating of type A (see table 1). (*a*) Maximum deformation as a function of Ca. (*b*, *c*) Deformation pattern as function of Ca for (*b*) fixed-contact-angle, (*c*) fixed-contact-points conditions. · · ·, Asymptotic solution (§3); ——, direction solution (§4).

antisymmetric while the flow pattern is symmetric. Small but finite values of Ca eliminate antisymmetry of the deformation and produce an asymmetric flow field.

4.2.7. *Reynolds number effects*

Figure 13 shows the evolution of the interface deformation subject to heating by a heat source (type C) as a function of the Reynolds number. It is shown that an increase of the Reynolds number from 0 to 20 increases the amplitude of the deformation by 50%. It can be concluded that the interface is very sensitive to convective effects, at least for certain types of external heating and in a certain range of cavity length. This issue is the subject of further investigations.

Thermocapillary convection at high Reynolds numbers has been studied previously by various authors with Re up 10^5 (Rivas & Ostrach 1989; Hadid & Roux 1990, 1992; Laure *et al.* 1990; Carpenter & Homsy 1990; Rivas 1991; Zebib *et al.* 1985; Cowley & Davis 1983) but always with the assumption of small (i.e. negligible) interface deformation. Results displayed in figure 13 show that the results available in literature should be treated with extreme caution owing to the possible occurrence of large interfacial distortions.

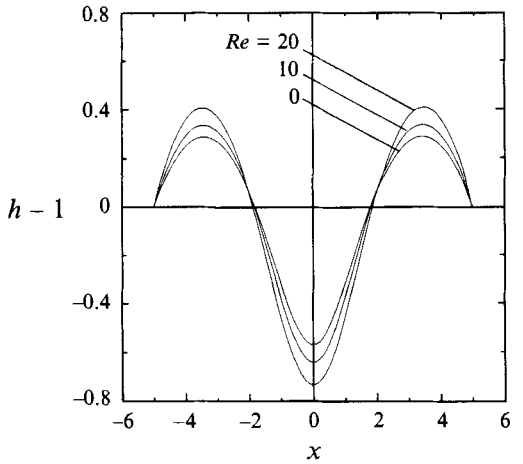

FIGURE 13. Interface deformation as function of Reynolds number. External heating of type C (see table 1). $Ma = 0$, $Bi = \infty$, $Ca = 0.024$, $L = 10$, $h(-\frac{1}{2}L) = h(\frac{1}{2}L) = 1$.

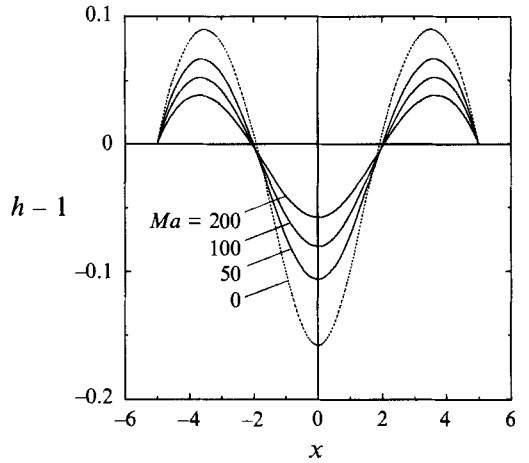

FIGURE 14. Interface deformation as function of Marangoni number. External heating of type C (see table 1). $Re = 0$, $Bi = 1$, $Ca = 0.024$, $L = 10$, $h(-\frac{1}{2}L) = h(\frac{1}{2}L) = 1$.

4.2.8. *Marangoni number effects*

Figure 14 shows the evolution of the interface deformation subject to heating by a heat source (type C) as a function of the Marangoni number for $Re = 0$ and $Bi = 1$. The results shown demonstrate a relative insensitivity of the interface distortion to convective heat transport. The maximum distortion decreases with an increase of Ma, which is due to a reduction of the effective temperature gradient along the interface.

5. Interface diagnostics

A direct relation between the external heating and the interface deformation cannot be established under general flow conditions. The occurrence of large deformation and, perhaps, breakup of the layer, can be predicted by carrying out a direct solution of the whole problem using the method described in §4.1. A cheaper alternative is offered by carrying out a solution with the small-deformation assumption, such as described in §3, and diagnosing the true behaviour of the interface by evaluating the integrals

appearing in (3.9) and (3.11*a*, *b*). A numerical solution of the Navier–Stokes equations still has to be carried out, but the geometry of the solution domain is simple and the location of the boundary conditions is fixed.

We shall begin discussion of the interface diagnostics by considering a cavity with fixed contact angles. Solution of the deformation equation (3.8*a*) with boundary conditions (4.2*a*) and volumetric constraint (4.15) results in

$$h_1(x) = x\int_{-L/2}^{x} W\,\mathrm{d}x - \int_{-L/2}^{x} xW\,\mathrm{d}x + \frac{1}{2}\int_{-L/2}^{L/2} xW\,\mathrm{d}x - \frac{1}{2L}\int_{-L/2}^{L/2} x^2 W\,\mathrm{d}x, \tag{5.1}$$

where $W(x)$ is defined by (3.8*e*). The additive pressure constant contained in $W(x)$ is evaluated as

$$B = \frac{1}{L}\int_{-L/2}^{L/2} [-\bar{p}_0(x,1) + 2v_{0y}(x,1)]\,\mathrm{d}x. \tag{5.2}$$

Construction of solution (5.1) shows that

$$I_1 = \int_{-L/2}^{L/2} W\,\mathrm{d}x$$

is always zero which leaves only

$$I_2 = \int_{-L/2}^{L/2} xW\,\mathrm{d}x \quad \text{and} \quad I_3 = \int_{-L/2}^{L/2} x^2 W\,\mathrm{d}x$$

available for diagnostic purposes. The utility of such diagnostics is demonstrated by results of calculations for temperature distributions A–E:

A: $I_3 = 0$, $I_2 = -4.49, -12.48, -24.47$ for $L = 6, 10, 14$;
B: $I_3 = 0$, $I_2 = -8.04, -26.95, -42.78$ for $L = 4, 6, 7$;
C: $I_2 = 0$, $I_3 = -17.69, -56.47, -117.9$ for $L = 4, 6, 8$;
D: $I_3 = 0$, $I_2 = -0.8066, -0.3934, -0.025$ for $L = 4, 6, 8$;
E: $I_3 = 0$, $I_2 = -1.434, -1.487, -1.449$ for $L = 4, 6, 8$.

The divergent behaviour of either I_2 or I_3 in cases that violate the existence conditions is clearly visible. The disappearance of either I_2 or I_3 in some of the above case studies in a result of symmetries present in the problem (Stokes flow) and does not indicate any general trend.

Solution of the small-deformation problem in the fixed-contact-point case results in

$$h_1(x) = x\int_{-L/2}^{x} W\,\mathrm{d}x - \int_{-L/2}^{x} xW\,\mathrm{d}x - \left(\frac{x}{2}+\frac{L}{4}\right)\int_{-L/2}^{L/2} W\,\mathrm{d}x + \left(\frac{x}{L}+\frac{1}{2}\right)\int_{-L/2}^{L/2} xW\,\mathrm{d}x \tag{5.3}$$

with the constant in the pressure field evaluated as

$$B = \frac{3}{2L}\int_{-L/2}^{L/2} \bar{W}\,\mathrm{d}x - \frac{6}{L^3}\int_{-L/2}^{L/2} x^2 \bar{W}\,\mathrm{d}x, \tag{5.4}$$

where $\bar{W}(x) = -\bar{p}_0(x,1) + 2v_{0y}(x,1)$. The diagnostic integrals can be evaluated (regardless of the pressure normalization used) as

$$I_1 = \int_{-L/2}^{L/2} W\,\mathrm{d}x = -\frac{1}{2}\int_{-L/2}^{L/2} \bar{W}\,\mathrm{d}x + \frac{6}{L^2}\int_{-L/2}^{L/2} x^2 \bar{W}\,\mathrm{d}x, \tag{5.5a}$$

$$I_2 = \int_{-L/2}^{L/2} W\,\mathrm{d}x = \int_{-L/2}^{L/2} x\bar{W}\,\mathrm{d}x \tag{5.5b}$$

$$I_3 = \int_{-L/2}^{L/2} x^2 W\,\mathrm{d}x = \frac{3}{2}\int_{-L/2}^{L/2} x^2 \bar{W}\,\mathrm{d}x\frac{L^2}{8} - \int_{-L/2}^{L/2} \bar{W}\,\mathrm{d}x. \tag{5.5c}$$

Results of calculations give for temperature distributions A–E:

A: $I_1 = I_3 = 0$, $I_2 = -12.48, -49.97, -112.5$ for $L = 10, 20, 30$;

B: $I_1 = I_3 = 0$, $I_2 = -8.04, -29.95, -63.86$ for $L = 4, 6, 8$;

C: $I_2 = 0$, $I_1 = -6.621, -9.412, -11.06$; $I_3 = -26.52, -84.71, -176.87$ for $L = 4, 6, 8$;

D: $I_1 = I_3 = 0$, $I_2 = --0.807, -0.393, -0.025$ for $L = 4, 6, 8$;

E: $I_1 = I_3 = 0$, $I_2 = -1.43, -1.49, -1.45$ for $L = 4, 6, 8$;

and show behaviour of I_1, I_2 and I_3 consistent with the existence condition (3.9) and (3.11*a*, *b*). Again, the disappearance of either (I_1, I_3) or I_2 results from symmetries present in the problem and does not indicate any general trend.

The above discussion shows that integrals I_1, I_2 and I_3 can be used for a relatively simple prediction of whether a particular heating can generate large distortions (and possible breakup) of the interface.

6. Conclusions

Analysis of thermocapillary effects in an infinite liquid layer in the absence of gravity was carried out. It was shown that the layer may exist only if the external temperature field satisfies restrictive existence conditions. The explicit form of these conditions was given in the case of negligible convective transport. The form of the existence conditions shows that it may not be possible to enforce them in the case of a general flow (i.e. with convective effects present).

Analysis of a finite layer subject to carefully selected types of external heating was also carried out. Results show that if the external temperature field does not satisfy the existence conditions determined in the case of an infinite layer, large interfacial deformations occur, leading to breakup of the layer if the cavity is made sufficiently long. Since the temperature fields satisfying the existence conditions are rather unusual, an experimenter should be prepared for the fact that a response of the layer to an external heating in the actual experiment might consist of large interfacial distortions and, possibly, breakup of the layer. An increase of the Reynolds number increases deformation and leads to an earlier breakup of the interface, while an increase of the Marangoni number reduces this deformation.

This work was supported by the NSERC of Canada.

Appendix A

Consider loading function $W(x)$ in the form

$$W(x) = -\frac{\sin(x)}{x} - 2\frac{\cos(x)}{x^2} + 2\frac{\sin(x)}{x^3} + 2\pi^{1/2}\mathrm{e}^{-x^2} - 4\pi^{1/2}x^2\mathrm{e}^{-x^2}. \tag{A 1}$$

Its double integration and application of conditions (3.8*b*, *d*) gives a deformation in the form

$$h_1(x) = \frac{\sin(x)}{x} - \pi^{1/2}\mathrm{e}^{-x^2}. \tag{A 2}$$

Function (A 1) does not satisfy condition (3.11), but the relevant integrals exist owing to oscillatory decay of $W(x)$ for $x \to \pm\infty$.

Appendix B

The governing equations (3.4) and boundary conditions (3.5*a*, *b*, *d*, *e*) reduce in the case of $Re = Ma = 0$ and $h_0 = 1$ to the following form:

$$u_{0x}+v_{0y}=0, \quad u_{0xx}+u_{0yy}=p_{0x}, \quad v_{0xx}+v_{0yy}=p_{0y}, \quad T_{0xx}+T_{0yy}=0; \tag{B 1a–d}$$

$$y=0: \quad u_0=v_0=T_{0y}=0, \tag{B 2a}$$

$$y=1: \quad v_0=0, \tag{B 2b}$$

$$u_{0y}=-T_{0x}, \quad T_{0y}+Bi(T_0-T_g)=0. \tag{B 2c, d}$$

To solve the system (B 1) and (B 2), we define the Fourier transform of $q(x, y)$ as

$$\hat{q}(k;z)=(2\pi)^{-1/2}\int_{-\infty}^{\infty} q(x,y)\,\mathrm{e}^{\mathrm{i}kx}\,\mathrm{d}x, \tag{B 3}$$

where q stands for any of u_0, v_0, p_0, T_0 and the hat denotes its Fourier transform. Transformation of (B 1) and (B 2), solution of the resulting system of ordinary differential equations in the Fourier space and transformation back into the physical space gives an explicit solution for all dependent variables in the form

$$T_0(x,y)=(2\pi)^{-1/2}\int_{-\infty}^{\infty}\hat{T}_0(k;y)\,\mathrm{e}^{-\mathrm{i}kx}\,\mathrm{d}k, \tag{B 4a}$$

$$u_0(x,y)=\mathrm{i}(2\pi)^{-1/2}\int_{-\infty}^{\infty}kf(k;y)\,\hat{T}_0(k;1)\,\mathrm{e}^{-\mathrm{i}kx}\,\mathrm{d}k, \tag{B 4b}$$

$$v_0(x,y)=(2\pi)^{-1/2}\int_{-\infty}^{\infty}g(k;y)\,\hat{T}_0(k;1)\,\mathrm{e}^{-\mathrm{i}kx}\,\mathrm{d}k, \tag{B 4c}$$

$$p_0(x,y)=-(2\pi)^{-1/2}\int_{-\infty}^{\infty}s(k;y)\,\hat{T}_0(k;1)\,\mathrm{e}^{-\mathrm{i}kx}\,\mathrm{d}k, \tag{B 4d}$$

where

$$\hat{T}_0(k;y)=\frac{Bi\hat{T}_g(k)\cosh(ky)}{k\sinh(k)+Bi\cosh(k)},$$

$$f(k;y)=k^{-1}\{[\tfrac{1}{2}+k\xi_1(k)(y-1)]\sinh[k(y-1)]$$
$$-[\xi_2(k)-\xi_1(k)-\tfrac{1}{2}k(y-1)]\cosh[k(y-1)]\},$$

$$g(k;y)=[\xi_2(k)-\tfrac{1}{2}k(y-1)]\sinh[k(y-1)]-k\xi_1(k)(y-1)\cosh[k(y-1)],$$

$$s(k;y)=k\sinh[k(y-1)]+2k\xi_1(k)\cosh[k(y-1)],$$

$$\xi_1(k)=\sinh^2(k)/[\sinh(2k)-2k], \quad \xi_2(k)=k^2/[\sinh(2k)-2k],$$

and i denotes the imaginary unit. The pressure p_0 is implicitly normalized by existence of its Fourier transform, i.e. $p_0\to 0$ as $x\to\pm\infty$.

The special case of periodic heating $T_g(x)=T_a\sin(\alpha x)$ results in a solution in the form

$$T_0(x,y)=\frac{T_a\,Bi\cosh(\alpha y)}{\alpha\sinh(\alpha)+Bi\cosh(\alpha)}\sinh(\alpha x), \tag{B 5a}$$

$$u_0(x,y)=-\bar{T}_a\,\alpha f(\alpha;y)\cos(\alpha x), \quad v_0(x,y)=\bar{T}_a\,g(\alpha;y)\sin(\alpha x), \tag{B 5b, c}$$

$$p_0(x,y)=-\bar{T}_a\,s(\alpha;y)\sin(\alpha x), \tag{B 5d}$$

where $$\bar{T}_a=T_a\,Bi\cosh(\alpha)/(\alpha\sinh(\alpha)+Bi\cosh(\alpha)).$$

REFERENCES

ADLER, J. & SOWERBY, L. 1970 *J. Fluid Mech.* **42**, 549.

BIRIKH, R. V. 1966 *J. Appl. Mech. Tech. Phys.* **3**, 69.

CARPENTER, B. & HOMSY, G. M. 1985 *J. Fluid Mech.* **155**, 429.

CARPENTER, B. M. & HOMSY, G. M. 1990 *Phys. Fluids* (A) **2**, 137.

CHEN, C. & FLORYAN, J. M. 1994 *J. Comput. Phys.* **111**, 183–193.

COWLEY, S. J. & DAVIS, S. H. 1983 *J. Fluid Mech.* **135**, 175.

FLORYAN, J. M. & KROL, S. 1991 *Adv. Space Res.* **11** (7), 125.

HADID, H. B. & ROUX, B. 1990 *J. Fluid Mech.* **221**, 77.

HADID, H. B. & ROUX, B. 1992 *J. Fluid Mech.* **235**, 1.

HOMSY, B. G. & MEIBURG, E. 1984 *J. Fluid Mech.* **139**, 443.

KOPBOSYNOV, B. K. & PUKHNACHEV, V. V. 1986 *Fluid Mech. – Sov. Res.* **15**, 95.

LAI, C. L. & CHAI, A. T. 1986 *Acta Astronautica* **13**, 655.

LAURE, P., ROUX, B. & HADID, H. B. 1990 *Phys. Fluids* A **2**, 516.

LEVICH, V. G. 1962 *Physicochemical Hydrodynamics.* Prentice-Hall.

PIMPUTKAR, S. M. & OSTRACH, S. 1980 *Phys. Fluids* **23**, 1281.

PSHENICHNIKOV, A. F. & TOKMENINA, G. A. 1983 *Izv. Akad. Nauk. SSSR Mekh. Zhid. Gaza* **3**, 150.

RIVAS, D. 1991 *Phys. Fluids* A **3**, 280.

RIVAS, D. & OSTRACH, S. 1989 *Physico Chem. Hydrodyn.* **11**, 765.

RYBICKI, A. & FLORYAN, J. M. 1987 *Phys. Fluids* **30**, 1956.

SANOCHKIN, YU. V. 1983 *Zh. Prikl. Mekh. Tekh. Fiz.* **6**, 134.

SANOCHKIN, YU. V. 1984 *Izv. Akad. Nauk. SSSR Mekh. Zhid. Gaza* **6**, 146.

SEN, A. K. 1986 *Phys. Fluids* **29**, 3881.

SEN, A. K. & DAVIS, S. H. 1982 *J. Fluid Mech.* **121**, 163.

TAN, M. J., BANKOFF, S. G. & DAVIS, S. H. 1990 *Phys. Fluids* A **2**, 313.

VYBORNOV, S. I. & SANOCHKIN, YU. V. 1985 *Izv. Akad. Nauk. SSSR. Mekh. Zhid. Gaza* **1**, 176.

YIH, C. S. 1968 *Phys. Fluids* **11**, 477.

ZEBIB, A., HOMSY, G. M. & MEIBURG, E. 1985 *Phys. Fluids* **28**, 3467.